SM 85-4-1

THE ROLE OF DAMAGE-SOFTENED MATERIAL BEHAVIOR IN THE FRACTURE OF COMPOSITES AND ADHESIVES

by

T. Ungsuwarungsri* and W.G. Knauss**

Graduate Aeronautical Laboratories
California Institute of Technology
Pasadena, CA 91125

* Graduate Research Assistant

** Professor of Aeronautics and Applied Mechanics

ABSTRACT

Failure mechanisms of materials under very high strains experienced at and ahead of the crack tip such as the formation, growth and interaction of microvoids in ductile materials, microcracks in brittle solids or crazes in polymers and adhesives are represented by one-dimensional, nonlinear stress-strain relations possessing different post-yield softening (strain-softening) behavior. These reflect different ways by which the material loses capacity to carry load up to fracture or total seperation. A DCB type specimen is considered in this study.[1] The nonlinear material is confined to a thin strip between the two elastic beams loaded by a wedge. The problem is first modelled as a beam on a nonlinear foundation. The pertinent equation is solved numerically as a two-point boundary value problem for both the stationary and the quasi-statically propagating crack. A finite element model is then used to model the problem in more detail in order to assess the adequacy of the beam model for the reduction of experimental data to determine in-situ properties of the thin interlayer.

It is found that the energy release rate derived by assuming built-in conditions at the crack tip can be used to calculate the fracture (surface) energy more accurately and conveniently than Berry's scheme [2] even in cases where the built-in assumption is apparently invalid. The analyses suggest that it is possible to infer from detailed macroscopic measurements of the deformations of the beam prior to and during crack growth the approximate characteristics of the complete (uniaxial) material stress-strain behavior of the cohesive interlayer including loading and strain-softening.[2]

1. This paper is a shortened version of reference 1.

2. An experimental program is being conducted in our laboratories to study the stress-strain characteristics of a number of polymeric solids using the DCB model discussed in this paper.

1. INTRODUCTION

The double cantilever beam (DCB) specimen has been used extensively in crack propagation studies due to its simple geometry which is attractive from both experimental and theoretical standpoints. Berry [3] investigated the implications of the Griffith fracture criterion for the DCB specimen and showed that for the built-in beam, fracture initiated when the moment at the crack tip reached a critical value. Bilek and Burns [4] in their dynamic analysis derived the same equations through the application of Hamilton's principle. Similar results were also obtained by Steverding and Lehnigk [5] using a different approach. Kanninen [6] employed the model of a beam on an elastic foundation to relax the built-in constraint and later [7] extended his analysis to the dynamic case introducing a Timoshenko beam on a generalized elastic foundation model to account for shear deformation and rotary inertia.

In the present work, we generalize the foundation to a nonlinear one characterized by an initially linear elastic stress-strain relation and an unloading tail reflecting loss of load carrying ability (strain-softening). Subsequently, fracture occurs at some critical strain at which the foundation stiffness drops to zero. Thus the model allows the crack to propagate without any additional prescription of a failure criterion, so that the nonlinear DCB analysis becomes a potential tool for determining the in-situ, nonlinear material characteristics of the bond-interlayer. As complete stress-strain characterizations of real materials are not yet available, we resort first to some idealized (hypothetical) material models in an attempt to extract from the solution of the problem certain measurable macroscopic quantities that might allow one to characterize the complete material behavior in the continuum sense: In this we assume that a sufficiently large number of microvoids, microcracks or craze fibrils are present in each small volume element under load at the "crack front" such that the damage-induced loss of load carrying capacity can be meaningfully averaged and represented as a continuum response. Studies involving porous and damaged materials are numerous, for instance

McClintock [8], Gurson [9] who developed approximate yield criteria and flow rules for dilatant ductile materials; Needleman [10], Berg [11] who proposed a continuum model for plastic deformation of microporous metal aggregates; Rice and Needleman [12] studied metals with constitutive dependence on hydrostatic stress (which promotes void nucleation and growth) in sheet metal forming processes; Krajcinovic [13] presented a constitutive model for material containing flat planar microcracks such as concrete; see also Dougill [14], Rudnicki [15] and Bazant [16]. In our studies we are primarily interested in the nonlinear response of homogeneous or multiphase polymers such as those used in advanced composites and adhesives.

To simulate crack propagation in our finite element study, we employ a scheme different from the ones proposed thus far. The usual node release methods proposed by Andersson [17], Kfouri & Miller [18], Rydholm et al. [19] and Malluck & King [20, 21] permit only a single node to be released at a time by reducing the reaction force at the crack tip node over several steps in some prescribed manners when a fracture criterion, such as a critical crack tip opening displacement (CTOD) or crack tip opening angle (CTOA), is reached. These methods require continual external monitoring and interruptions of the computations which become very time-consuming and inconvenient for simulation of crack growth over distances of ten or more elements. Hoff et al. [22] introduced a technique employing spring and gap elements to circumvent this problem, the method requires a subroutine to control the openings of the gap elements and thus does not put crack propagation under total control of the external loadings. In this study, we use nonlinear springs that have no restraining forces beyond a certain critical strain to imitate the failure characteristics of the cohesive material in the interlayer. Thus when a nonlinear spring joining a node along the crack path to the foundation 'fails', a node is released and the crack advances. In this way, crack propagations over distances of tens of elements (or more) are easily simulated requiring no external monitoring whatsoever.

The present problem is considered as a precursor to the more general one wherein a yield criterion based on a strain softening material is used. In that more general case one needs to be concerned with the highly triaxial stress state at the crack tip as well as with the consequences of locally unstable material behavior on global stability. In cases where the process zone is 'narrow' compared to the size of the specimen considered, a 'boundary layer' type model in which the damage-softened material behavior is confined to a thin layer adjacent to the crack plane may prove to be a realistic and yet computationally inexpensive scheme for studying crack growth. Certain rubber-toughened materials seem to obey this model very closely. Much work remains before the appropriate continuum models for enigneering materials of interest are experimentally identified and numerically verified under a wide range of loading conditions.

In the next section, we discuss the problem of the beam on a nonlinear foundation, its numerical solution schemes and the results for both stationary and propagating[3] cracks. The finite element model is presented in Section 3 and is followed by comparisons with the beam equation model in Section 4. Applications of the findings are demonstrated in Section 5, with conclusions summarized in Section 6.

2. THE BEAM ON A NONLINEAR FOUNDATION MODEL

The model and relevant geometric and material definitions are depicted in Figure 1. We start with the equation for a Bernoulli-Euler beam (with constant EI) resting on a nonlinear foundation

$$EI \frac{d^4w}{dx^4} + q(w) = 0 \qquad (2.1)$$

where E is the Young's modulus of the beam, $I = \frac{1}{12}bh^3$ (for rectangular

3. In the present investigation, no inertia (dynamic) effects are considered, therefore 'propagation' refers to 'quasi-static' propagation throughout.

cross section); b and h are the width and height of the beam, respectively, w is the vertical displacement of the beam neutral axis, and q(w) the nonlinear restoring force per unit length of the foundation. We consider q(w) such that, typically, the small strain response corresponds to an "elasticity" modulus that is approximately an order of magnitude smaller than that of the beam.

Equation (2.1) is to be solved subject to boundary conditions at the loading end and at a distance far away from the loading end where the conditions are those of a semi-infinite beam on a linearly elastic foundation. This may always be assumed if the 'uncracked portion' of the beam is longer than two to three times the exponential decay length ($1/\beta$; see equation (2.2)).

2.1. Solution Schemes.

The equation to be solved is nonlinear and involves boundary conditions at two points. A standard technique is the shooting method [23], which seeks the proper boundary conditions at one end point that also satisfy the boundary conditions at the other end point by Newton's iteration based on the Jacobian matrix formed by the miss-hits at the other end point and the current boundary conditions chosen at the first end point. The usual difficulty encountered is in obtaining convergence without requiring an excessive number of iterations; the rate of convergence depends strongly on the proximity of the initial guess of the boundary conditions at the first end point to the correct boundary conditions.

In the present problem, we take advantage of the existence of the solution for the beam on a linear foundation by starting the integration from the region where the foundation response is linear and an analytical solution is available. We integrate numerically up to the crack tip beyond which the beam is free of surface tractions except for the very end. For this unloaded section a simple beam solution can again be exploited. For convenience we set up our coordinate system as shown in

Figure 2.

The solution for a semi-infinite beam on an elastic foundation (i.e., q(w)=kw in (2.1)) with boundary conditions

$$w(\infty) = w'(\infty) = w''(\infty) = w'''(\infty) = 0$$

is of the form

$$w(x) = e^{-\beta x}(A\cos\beta x + B\sin\beta x) \tag{2.2}$$

where $\beta = \left[\frac{k}{4EI}\right]^{\frac{1}{4}}$ and A, B = constants.

To start the integration of equation (2.1) from the elastic foundation region, we observe that the choice of the starting point is arbitrary; for convenience we may, therefore, choose x to be zero such that

$$w(0) = w_o \tag{2.3a}$$

$$w'(0) = 0 \tag{2.3b}$$

which yields $A = B = w_o$ and

$$w''(0) = -2\beta^2 w_o \tag{2.3c}$$

$$w'''(0) = 4\beta^3 w_o \tag{2.3d}$$

Note that it is fastest to integrate from $w_o < 0$ into the nonlinear region (see Figure 2), and that w_o has to be such that no yielding occurs in compression at the starting point x = 0. In this work, we assume that the yield strain in compression is equal to the yield strain in tension. It should be pointed out that by starting the integration from conditions derived from (2.2), we are guaranteed an exponentially decaying solution

as $x \to +\infty$; this would not necessarily be the case if one were to start the integration from the loading end as any small error in the initial guess could cause the components of solution with terms proportional to $e^{\beta x}$ to enter and make the solution unbounded as $x \to +\infty$. Thus a poor initial guess at the loading end could result in extremely slow convergence or no convergence at all.

2.1.1. Stationary (Non-propagating) Case. For this case we seek the solution for a geometry with a pre-cut crack of length l under increasing load P to the point where crack propagation is imminent.

We obtain the solution by integrating[4] until $\frac{M}{P} = \frac{-M}{S} = l$ (with less than 0.1% error), here S is the shear for the free part of the beam, P is the end load, and M is the moment. We then obtain the rest of the solution from (see Figure 2)

$$\delta = \frac{Pl^3}{3EI} + |w'_t|l + w_t \tag{2.4}$$

where w_t is the displacement at the "crack tip"; $w_t \leq w_c$, and $|w'_t|$ is the slope of the neutral axis at the crack tip. When $w_t = w_c$, we reach the instant at which the crack is about to grow.

2.1.2. Quasi-static Propagation Case. Here the scheme is to integrate along x until $w = w_c$ (with less than 0.001% error) and then calculate the corresponding crack length and end conditions from: (see Figure 2)

$$P = -S_c,$$

$$l = \frac{M_c}{P},$$

$$\delta = \frac{Pl^3}{3EI} + |w'_c|l + w_c \tag{2.5}$$

---

4. The subroutine MODDEQ of the Caltech Computing Center which employs the Runge-Kutta-Gill method is used to solve a system of four first-order differential equations equivalent to equation (2.1).

where S_c and M_c are the shear and moment in the beam at the crack tip, and $|w_c'|$ is the slope of the beam there.

Other quantities such as the bending energy in the beam, E_b , the total work done, W, the work done on the interlayer, W_c , the size of the yield zone, $\alpha = |x_c - x_y|$, and the 'secant' compliance, $C \equiv \delta/p$, are readily computed. Note that for a nonlinear system, such as the one we are dealing with, it is appropriate to define the compliance C as $C \equiv \frac{d\delta}{dP}$; however in the present study, we intend to compare our results with previous findings in other studies where C has always been defined as the secant compliance which, strictly speaking, is only correct for linear systems. As there is no obvious advantage in employing the more general definition here, the usual definition is used.

2.2. Nondimensionalization.

For presentation of the results it is useful to non-dimensionalize pertinent parameters. We choose the thickness 'd' of the cohesive interlayer as the natural length scale, i.e., define

$$w^* \equiv \frac{w}{d}, \quad x^* \equiv \frac{x}{d}$$

Equation (2.1) is then reduced to[5]

$$w^{*(4)} + C_1 w^* = 0, \tag{2.1a}$$

with

$$C_1 \equiv 12 \left\{\frac{E_c}{E}\right\} \left\{\frac{d}{h}\right\}^3$$

where E_c is the elastic (small strain) modulus of the cohesive foundation.

5. See reference 1 for detail.

We summarize here other relevant dimensionless quantities for future reference:

$$\delta^* \equiv \delta/d, \qquad l^* \equiv l/d, \qquad h^* \equiv h/d, \qquad b^* \equiv b/d$$

$$q^* \equiv \frac{qd^3}{EI}, \qquad P^* \equiv \frac{Pd^2}{EI}, \qquad M^* \equiv \frac{Md}{EI}, \qquad C^* \equiv \frac{\delta^*}{P^*}$$

and $\gamma^* \equiv \frac{\gamma d^3}{EI}$ is the non-dimensionalized fracture energy (= area under the q-w curve).

2.3. Results and Discussions.

We present next results for the stationary crack and the propagating crack. The material models considered for the interlayer are all piecewise-linear and possess the same fracture energy. The following set of data is used throughout: E is chosen as the Young's modulus for Aluminum 2024 (10.6×10^6 psi). E_c, the small strain modulus of the cohesive interlayer, is taken to be 1.41×10^5 psi.[6] Also $h^* = h/d = 10.0$. These yield, $C_1 = 1.6 \times 10^{-4}$. The material models are[7] shown in Figure 3. They are intended to examine the effects of various nonlinear material characteristics on the measurable macroscopic quantities.

2.3.1. The Stationary Crack. In the following, the crack length is ten times the height of the beam. These results are presented in Figures 4-7. In Figure 4, the dashed lines exhibit the effects of the high compliance due to an initial low foundation resistance which subsequently increases and becomes fairly constant as the yield zone, α^*, grows. (Thus the compliance decreases and then levels off.) These dashed portions are

6. Note that E_c is about two order of magnitude smaller than E. If E_c is greater than a few percent of E, the beam may deform plastically near the crack tip rendering the present beam equation model inadequate.

7. The solution technique is capable of handling generally nonlinear q(w), even though we only consider here piecewise-linear material models.

approximately extrapolated based on the compliance values from Figures 5. Clearly, the existence and the gradient of an softening tail (as in materials 2 & 3) can be easily identified in any of these five plots as the onset of crack growth is approached, i.e., as $w_t^* \to w_c^*$. This fact may be used to approximately characterize q(w) from experimental data. In general, the compliance, C^*, the slope at the crack tip, $-w_t^{*\prime}$, and the size of the yield zone, α^*, are all monotonically increasing functions of w_c^*.

We shall discuss the application of this finding in connection with the characterization of q(w) in more detail in Section 5.2.

2.3.2. The Quasi-statically Propagating Crack. Before dealing with the nonlinear case we consider first certain results for the idealized situation where neither the interlayer nor the elasticity of the beam allows rotation of the 'built-in' end. We first derive the equations mentioned in Section 1 for the built-in beam case. Here the coordinate system is such that the load P is applied at x = 0, w(o) = δ and w(l) = w'(l) = 0. We have for this "idealized" case,

$$\delta = \frac{Pl^3}{3EI} \tag{2.6}$$

and for the bending energy in the beam U_b ,

$$U_b = \int_o^l \frac{M^2(x)}{2EI}dx = \frac{P^2}{2EI}\int_o^l x^2dx = \frac{P^2l^3}{6EI} \tag{2.7}$$

Griffith Condition: The energy release rate, G, is obtained from the potential energy Π of the system (both beams of the DCB specimen considered and hence the factor two) as follows

$$G = -\frac{\partial \Pi}{\partial l} = -\frac{\partial}{\partial l}2[U_b - P\delta] = -\frac{\partial}{\partial l}(-2\cdot\frac{P^2l^3}{6EI}) = \frac{P^2l^2}{EI} = 2\gamma b$$

Hence the moment at the crack tip required for crack growth M_c is

$$M_c = Pl = \sqrt{2EI\gamma b} \tag{2.8}$$

Combining (2.6) and (2.8), one finds

$$3P^2\delta = (2\gamma b)^{3/2} \sqrt{EI}. \tag{2.9}$$

Rewriting (2.9), one obtains

$$2\gamma = \frac{1}{b}\left\{\frac{(3P^2\delta)^2}{EI}\right\}^{1/3} . \tag{2.10}$$

In order to study how a certain quantity changes as the crack propagates quasi-statically, we denote the derivative with respect to crack length l by $\frac{d(\ )}{dl}|_{qs}$. Note that P is not constant as l increases but decreases such that quasi-static crack growth is maintained. Adopting this convention and using (2.7) and (2.8), there follows for the bending energy of the beam (here only half of the DCB specimen is considered)

$$U_b = \frac{M_c^2 l}{6EI} = (\frac{\gamma b}{3})l,$$

whence

$$\frac{dU_b}{dl}|_{qs} = \frac{\gamma b}{3} \tag{2.11}$$

For this ideal case, the rate of work done against interface forces as the crack propagates is

$$\frac{dW_c}{dl}|_{qs} = \gamma b \tag{2.12}$$

where W_c denotes the energy dissipated in the interlayer. Let W be the total work done by P, i.e., $W = \int_0^\delta P d\delta$, or $dW = Pd\delta$. Then in view of (2.6) and (2.8)

$$\frac{d\delta}{dl}\Big|_{qs} = \frac{2M_c l}{3EI}$$

so that

$$\frac{dW}{dl}\Big|_{qs} = P\frac{d\delta}{dl}\Big|_{qs} = \frac{2M_c Pl}{3EI} = \frac{2M_c^2}{3EI}.$$

In view of (2.8),

$$\frac{dW}{dl}\Big|_{qs} = \frac{4}{3}\gamma b \tag{2.13}$$

Combining (2.11), (2.12), and (2.13) yields

$$\frac{dU_b}{dl}\Big|_{qs} = \frac{1}{4}\frac{dW}{dl}\Big|_{qs}$$

$$\frac{dW_c}{dl}\Big|_{qs} = \frac{3}{4}\frac{dW}{dl}\Big|_{qs} \tag{2.14}$$

Thus for the idealized (built-in) case, 25% of the total work done is stored in the beam as bending energy while 75% is dissipated as fracture energy at the interface. Note in passing that in this idealized case the stress intensity factor is

$$K_I = (2\sqrt{3}h^{-3/2})Pl = (2\sqrt{3}h^{-3/2})M_c \tag{2.15}$$

But by (2.8), $M_c = f(\gamma, EI)$, therefore K_I at fracture is a constant as is G (the energy release rate).

Having considered this ideal case we consider now the situation where the nonlinear foundation allows both the displacement and the slope at the crack tip to be different from zero. The numerical results[8] in Figure 8 show that the P-δ relation depends only on γ and EI as suggested by

8. Here material #2 was not investigated, as we did not expect the use of its characteristic to contribute any additional insight into the problem.

equation (2.9) derived for the idealized case. Figure 9 indicates that M_c^* depends weakly on w_c^* and on the existence of a strain softening tail. The slope at the crack tip, $-w_c^{*\prime}$, increases and rapidly approaches an asymptotic value as the crack grows. The yield zone size α^* is shown to decrease and becomes constant as l^*/h^* increases.[9] In Figure 10, $P^*\delta^{*\frac{1}{2}}$ is shown to approach a constant value as l^*/h^* increases. In view of equation (2.9) and the behavior of $P^*\delta^{*\frac{1}{2}}$ exhibited in Figure 10, it seems possible that the fracture energy γ in the case where the beam supports rotates may still be approximated by equations of the same form as (2.10) and (2.10a). With this in mind, define

$$2\tilde{\gamma} \equiv \frac{1}{b}\left\{\frac{(3P^2\delta)^2}{EI}\right\}^{1/3} \tag{2.16}$$

$$2\tilde{\gamma}^* \equiv \frac{1}{b^*}(3P^{*2}\delta^*)^{2/3} \tag{2.16a}$$

In Figure 14, we compare the value of $\tilde{\gamma}^*$, the fracture (surface) energy as computed from equation (2.16a), to the exact value γ^* as calculated from the area under the q-w curve of the input data. Note that the vertical ordinates in Figures 13 and 14 encompass very narrow ranges of values.[10]

In these non-ideal cases, it is found that equations (2.9)-(2.14) remain valid with small errors which decrease rapidly with increasing crack length. The reason for this behavior is that the crack propagation has reached an asymptotic condition in the sense that neither α nor $-w_c^{\prime}$ is changing much. To see this consider the following argument:

For the idealized case, equation (2.10) can be written in functional form as

---

9. For quantitative display, see reference 1.

10. The accuracy of these results is demonstrated quantitatively in reference 22.

$$F(P, \delta, \gamma, EI) = 0 \qquad (2.17)$$

Note that the crack length l does not appear explicitly as it is already fixed through the equilibrium condition by specifying both P and δ. In the event that the support rotates (the nonlinear foundation case), the only additional physical parameter[11] which could be involved in (2.17) is w_c', however $\frac{dw_c'}{dl}|_{qs} << 1$ for $l/h \geq 5$ (see Figure 11). Thus, the slope at the crack tip hardly changes as the crack propagates and, therefore, (2.17) still holds with good approximation for $l/h \geq 5$.

One could also think of the built-in case as a special case where $q(w) = \gamma\delta(w)$ = a delta function of integral measure γ and $w_c' = \alpha = 0$. Thus, for general q(w), one only needs to reach the asymptotic conditions for a long crack when w_c' and α are approximately constant for equation (2.17) to hold.

3. FINITE ELEMENT MODEL

The finite element program ABAQUS (version 4) running on a VAX-11/780 was used to model the beam and the nonlinear foundation. We use 4-noded bilinear plane elements to model the beam, and nonlinear springs restraining vertical motion of the beam to model the foundation. The 4-noded element is chosen for convenience in discretizing the foundation and in interpolating to locate the crack tip. The force-displacement relations of the nonlinear springs are patterned precisely after the material models shown in Figure 3.

---

11. Note that we may disregard w_c as an additional parameter since it is a constant for a given q(w) under consideration. It should also be pointed out that in all cases considered $|w_c'|$ is very small (≤ 0.014) i.e. less than 0.80^o in rotation at the crack tip, but the contribution of this small slope to the end displacement δ is not at all negligible, for instance, by equation (2.5) for $l/h = 10$, $h/d = 10$; $|w_c'|l = 0.3\delta$.

The discretization of the foundation is accomplished by attaching two identical nonlinear springs with total restraining forces equal to that of a continuous foundation to the bottom two nodes of each element of the beam at the interface. (For 8-noded biquadratic elements, this simple scheme would not work.)

The three meshes used for the beam are shown in Figure 12. Mesh #1 has 402 elements, 67 springs, 476 nodes, and a total of 952 degrees of freedom with the smallest element size of 0.1h × 0.05h. Mesh #2 has 540 elements, 90 springs, 637 nodes, and 1274 degrees of freedom with the same smallest element size as Mesh #1. Mesh #3 has 480 elements, 120 springs, 605 nodes and 1210 degrees of freedom with smallest element size of 0.25h × 0.1h. (For Mesh #2, an iteration takes approximately 75 CPU seconds and each increment requires 2 or 3 iterations.)

Mesh #1 is designed to capture the displacement details around the crack tip for $l^*/h^* = 10.0$ while mesh #2 is intended to study a shorter specimen and shorter crack lengths, i.e., $l^*/h^* \leq 3.5$. Mesh #3 is a more uniform mesh than the previous two and gives better results for a larger range of l^*/h^* (from 0.0 to 10.5).

The loading is achieved by prescribing the end displacement (δ) at the first node on the bottom line of the beam; the reaction force is then equal to P. The crack length is obtained by linear interpolation between a node where $w > w_c$ and an adjacent node where $w < w_c$. (This convenience would be lost if 8-noded biquadratic elements were used.) Convergence is considered attained when the forces at all nodes except those with prescribed displacements fall below 0.2% of the typical applied force values (in this case P). Since the beam is linearly elastic and the non-linear springs simply supply the proper boundary conditions, the typical residuals for the convergent solutions are $= 10^{-14}$ P which were much smaller than the set tolerance.

4. COMPARISONS OF THE BEAM MODEL WITH FINITE ELEMENT RESULTS

In this section, we examine the effects of including shear deformations through the finite element model while neglecting them in the beam equation model. The finite element results show that, excepting the beam end where the point force is applied, the stress components σ_{12} and σ_{22} in the beam are always less than 10% of the maximum value of σ_{11}. The maximum equivalent (von Mises) stress in the beam only reaches 53% of the yield stress σ_y (for Aluminum 2024, $\sigma_y = 50. \times 10^3$ psi). For beam materials with a low yield stress one must ensure that no yielding occurs in order for the present analysis to be applicable.

All comparisons shown here are for material model 3 (see Figure 3). First, the displacement contours of the top, center and bottom of the beam are compared with the solution to the beam equation (the neutral axis or center line displacement) at the same crack length to determine whether measurments can be taken at the top of a DCB specimen instead of at the bottom (interlayer) where it would be more difficult to measure; Figures 13 gives the <u>percent</u> differences of the two results. It is seen that the calculated displacements at the top, center or bottom of the beam are virtually identical; this is true as long as plastic deformations are absent. Thus the beam equation model yields results within a few percent of the finite element analysis for most of the length of the beam except at locations ahead of the crack tip. In that region ($x^*/h^* > 11.0$) w^* is very small and the mesh for the finite element analysis becomes coarse thus causing the percent error to rise.

The $P^*-\delta^*$ relationships obtained from both methods are compared in Figure 14. The finite element results for Mesh #2 and #3 give also the $P^*-\delta^*$ points before crack propagation commences (the peak in the upper left hand corner). The best agreement is obtained by using a uniform mesh (#3).

5. APPLICATIONS

We discuss next two practical applications of the findings, one is a rational method for determining the fracture surface energy, the other which is the primary goal of this study, namely, the rough characterization of q(w).

5.1. Determination of the Surface Energy.

In order to assess the delamination strength of composites or the strength of adhesives, it is desirable to determine the energy expended in causing crack propagation per unit of failure surface. Because of its relative simplicity the cleavage or double-cantilever-beam (DCB) specimen is often employed for this purpose. It has long been recognized that the simple formula derived on the basis of a built-in condition at the crack tip (see Section 2.3.2 and equation (2.16)) is not necessarily applicable when the rotation (slope) at the crack tip is nonzero. To circumvent this difficulty, Berry [2] introduced an ad hoc power-law scheme which is purported to be more accurate than the equation (2.16). However, as the results for the propagating crack in Section 2.3.2 suggest (see Figure 14), equation (2.16) can be used to calculate γ ($= \tilde{\gamma}$) conveniently and accurately.

We believe that the application of equation (2.16) is a more rational method for the determination of the surface energy than Berry's scheme which has been widely accepted. In the following, we will show numerically that Berry's scheme is an approximation to the results obtained through the solution of the beam equation with the finite rotation at the crack tip incorporated through the specification of q(w).[12] We start by outlining both schemes.

12. Note that regardless of the detailed characteristics of q(w), a finite rotation (slope) always exists at the crack tip and that this rotation contributes substantially to the end displacement as indicated in footnote 11.

Method (A): Berry [2] asssumes that the compliance is a power-law function of the crack length, l, in the form

$$C \equiv \frac{\delta}{P} = a l^N$$

where a depends on EI. Upon plotting log C versus log l and determining the slope N, one finds the energy release rate G to be

$$G = 2\gamma b = \frac{NP\delta}{l}$$

Let us adopt the notations (superscripts refer to method A)

$$G^{(A)} = 2\gamma^{(A)}b = \frac{NP\delta}{l} \tag{5.1}$$

Thus one needs to measure several sets of P,δ and l to be able to determine N resonably accurately from the plot of log C versus log l.

Method (B): The method proposed here is the application of equation (2.16),[13] i.e., we let,

$$G^{(B)} \equiv 2\gamma^{(B)}b \equiv \left\{\frac{(3P^2\delta)^2}{EI}\right\}^{1/3} \tag{5.2}$$

where $\gamma^{(B)} = \tilde{\gamma}$ defined by (2.16). Both schemes are applied to experimental data on composite delamination taken from reference 26 and are compared in Table I.

13. This method was proposed and used earlier in [24,25] for cases where the 'built-in' conditions are assumed to be valid.

Table I

Material: Unidirectional Composite T300/5208, $E = 1.9 \times 10^7$ psi.
$N = 2.68$, (N is obtained from the plot of log C versus log l).
$h = 0.119$ in., $b = 0.205$ in., $EI = 547.0$ lb-in^2

l/h	P(lb)	l(in)	δ(in)	$2\gamma^{(A)}$	$2\gamma^{(B)}$	$\frac{2\gamma^{(A)}}{2\gamma^{(B)}}$
22.3	3.05	2.65	0.105	1.58	1.22	1.30
24.9	3.12	2.96	0.135	1.86	1.49	1.25
33.8	2.31	4.02	0.220	1.65	1.38	1.20
44.9	1.75	5.34	0.375	1.61	1.36	1.18
47.6	1.82	5.67	0.425	1.78	1.56	1.14
52.5	1.50	6.25	0.480	1.51	1.31	1.15
56.9	1.42	6.77	0.540	1.48	1.31	1.13
62.8	1.37	7.47	0.690	1.65	1.47	1.12
			$2\gamma_{ave.}$ (lb/in)	1.65	1.39	
			Standard Deviation	0.12	0.10	

One notes from Table I that the results for γ based on Berry's scheme (Method A) are consistently higher than for the scheme proposed here (Method B) by roughly 20% on the average. The question now arises whether one method yields a better estimate for γ than the other.

Without knowing from another independent source a very reliable value of γ, we resort to an indirect argument based on the numerical solutions for the model of a beam on a nonlinear foundation. To do this, we calculate N numerically as a function of l^*/h^* by following Method (A).[14] If Berry's assumption is correct, N should be nearly constant. As depicted in Figure 15, N increases with l^*/h^* and approaches $N = 3$ which

14. The values of N are the local slopes of the log C versus log l plot.

corresponds to the idealized case (see equation (2.6)) as $l^*/h^* \to \infty$. It is evident that N varies considerably for all three material models studied especially for shorter crack lengths. Therefore the value of N obtained using Berry's scheme is simply an approximation.

The fact that we find N in Berry's method to be a function of l indicates that the power law assumption is not really acceptable (since an analytical basis is lacking in the first place) and that the proposed method (B), allowing for the rotation of the 'beam end', is inherently more rational.[15]

To further confirm the above point, we list values of $\frac{G^{(B)}}{G^{(A)}} = \frac{2\gamma^{(B)}}{2\gamma^{(A)}}$ in the last column of Table I. The surprisingly monotonic decreasing trend with increasing l^* of the above ratio in the data suggests that a high value for N (N = 2.68) was obtained from the log C versus log l plot. This high value for N corresponds to a rather long crack length (see Figure 15), and would thus yield an over estimate for γ for shorter crack length l since N is assumed to be constant in equation (5.1). This above discussion explains the decreasing trend in the ratio in the last column, since for longer crack lengths l, this high value N becomes closer to the proper local values of N's that would theoretically yield the correct value for γ.[16]

15. It turns out that even if one uses a continuously varying N for calculating γ through equation (5.1), the results are still less accurate than the simple application of equation (5.2). See reference 1 for quantitative details.

16. This comparison was made on two sets of experiments which yielded the same qualitative results, see reference 1 for more detail. The experiments from which the data are taken were carried out on nonsymmetric DCB specimens, i.e., the heights of the two beams were not always equal; we assume δ to be the average of the sum of the δ's of each beam. Details are given in reference 26.

5.2. Characterization of q(w).

We next discuss how the nonlinear characteristics of q(w) may be estimated based on information gathered from basic material testings and tests on DCB specimens. The properties of q(w) which are of interest are E_c, w_y, w_c, γ as well as the existence and gradient of an unloading tail. We outline below the methodology by which the characterization may proceed:

a. E_c and w_y can be determined from uniaxial tests.

b. w_c may be obtained from ultimate strain tension tests or optical measurements of the displacement contour from the DCB specimen tests.[17]

c. γ is easily computed using equation (2.16) or equation (5.2) as discussed at length in Section 5.1.

d. The existence and the gradient of an unloading tail can be identified and estimated by plotting C, w_t, $-w_t'$ and α as a function of P using DCB specimen test results for the stationary crack case (see Section 2.3.1, Figures 5-7).

These determinations are sufficient to provide a bound on the shape of the function q(w). Refinements of this approximate characterization can then be obtained by solving[18] the beam equation for various assumed q(w)'s (within the above bound) to better match experimental results.

---

17. Note that from results depicted in Figure 16, the displacement profile can be conveniently taken at the top surface of the beam since it is virtually identical to the profiles at the center and bottom surface of the beam (as long as there is no plastic deformation).

18. We mention in passing that the solutions of the beam equation are relatively inexpensive compared to the finite element solutions.

6. CONCLUDING REMARKS

We have established a possible experimental-analytical procedure by which certain nonlinear (cohesive) material characteristics may be determined approximately. In addition, a rational method for determining the surface (or fracture) energy in DCB specimen tests which accounts for the rotation at the crack tip ('built-in' end) and supplants Berry's method is proposed.

7. ACKNOWLEDGEMENTS

This work formed a preliminary study on the role of strain-softening characteristics of matrix materials in the fracture of composites. It was supported by the National Aeronautics and Space Administration under the technical monitorship of Dr. John H. Crews (Grant No. NAG-1-474). The finite element work was sponsored by the Air Force Office of Scientific Research through Grant No. AFOSR-84-0254. We are also grateful to Hibbitt, Karlsson & Sorensen, Inc. for making available the ABAQUS finite element code under an academic license.

8. REFERENCES

1. Ungsuwarungsri, T., "The Effect of Strain-Softening Cohesive Material on Crack Stability," Ph.D. Thesis, Graduate Aeronautical Laboratories, California Institute of Technology, Pasadena (1986) 1-75.

2. Berry, J.P., Journal of Applied Physics 34 (1963) 62-68.

3. Berry, J.P., Journal of the Mechanics and Physics of Solids 8 (1960) 194-216.

4. Bilek, Z.J. and Burns, S.J., Journal of the Mechanics and Physics of Solids 22 (1974) 85-95.

5. Steverding, B. and Lehnigk, S.H., International Journal of Fracture 6 (1970) 223-232.

6. Kanninen, M.F., International Journal of Fracture 9 (1973) 83-92.

7. Kanninen, M.F., International Journal of Fracture 10 (1974) 415-430.

8. McClintock, F.A., Journal of Applied Mechanics 35 (1968) 363-371.

9. Gurson, A.L., Journal of Engineering Materials and Technology 99 (1977) 2-15.

10. Needleman, A., Journal of Applied Mechanics 39 (1972) 964-970.

11. Berg, C.A., Inelastic Behavior of Solids, M.F. Kanninen et al. (Editors), McGraw Hill, New York (1970) 171-209.

12. Rice, J.R. and Needleman, A., Mechanics of Sheet Metal Forming, D.P. Koistinen and N.M. Wang (Editors), Plenum, New York (1978) 237-267.

13. Krajcinovic, D., Journal of Applied Mechanics 50 (1983) 355-360.

14. Dougill, J.W., Journal of Applied Mathematics and Physics (ZAMP), 27 (1976) 423-436.

15. Rudnicki, J.W., Journal of Rheology 28 (1984) 759-778.

16. Bazant, Z.P., International Journal of Solids and Structures, 16 (1980) 873-901.

17. Andersson, H., Journal of the Mechanics and Physics of Solids 21 (1973) 337-356.

18. Kfouri, A.P. and Miller, K.J., Proceedings of the Institution of Mechanical Engineers (London), 190 (1976) 571-584.

19. Rydholm, G., Fredricksson, B. and Nilsson, F., Numerical Methods in Fracture Mechanics, A.R. Luxmoore and D.R.J. Owen (Editors), University College of Swansea, Swansea, Wales (1978) 660-672.

20. Malluck, J.F. and King, W.W., Numerical Methods in Fracture Mechanics, A.R. Luxmoore and D.R.J. Owen (Editors), University College of Swansea, Swansea, Wales (1978) 648-659.

21. Malluck, J.F. and King, W.W., Crack Arrest Methodology and Applications, G.T. Hahn and M.F. Kanninen (Editors), ASTM STP 711 (1980) 38-53.

22. Hoff, R., Rubin, C.A., and Hahn, G.T., Engineering Fracture Mechanics 23 (1986) 105-118.

23. Keller, H.B., "Numerical Solution of Two Point Boundary Value Problems," Series: Regional Conference in Applied Mathematics, SIAM, 24 (1976).

24. Asbeck, W.K., Adhesion and Cohesion, P. Weiss (Editor), Elsevier Publishing, Amsterdam (1962) 101-120.

25. Malyshev, B.M. and Salganik, R.L., International Journal of Fracture 1 (1965) 114-128.

26. Chai, H., "The Growth of Impact Damage in Compressively Loaded Laminates," Ph.D. Thesis, Graduate Aeronautical Laboratories, California

Institute of Technology, Pasadena (1982) 102-126.

9. FIGURE CAPTIONS

Figure 1. Problem definition of the geometry and material parameters.

Figure 2. Solution schemes.

Figure 3. Material models (1, 2, 3 and 4).

Figure 4. End load versus end displacement for the stationary crack (material models 1, 2, 3, and 4 as indicated). For explanation of the dashed portions of the P-δ curves see text.

Figure 5. Compliance as a function of the end load for the stationary crack (material models 1, 2, 3 and 4 as indicated).

Figure 6. Crack tip displacement as a function of the end load for the stationary crack (material models 1, 2, 3 and 4 as indicated).

Figure 7. Slope at the crack tip as a function of the end load for the stationary crack (material models 1, 2, 3 and 4 as indicated).

Figure 8. End load versus end displacement for the propagating crack (material models 1, 3 and 4 as indicated). Note that the relation displayed is not affected by the detailed characteristics of q(w).

Figure 9. Moment at the crack tip as a function of crack length for the propagating crack (material models 1, 3 and 4 as indicated).

Figure 10. $P^*\delta^{*\frac{1}{2}}$ as a function of crack length for the propagating crack (material models 1, 3 and 4 as indicated).

Figure 11. $\tilde{\gamma}^*/\gamma^*$ as a function of crack length for the propagating crack (Material models 1, 3 and 4 as indicated)

Figure 12. Finite element meshes.

Figure 13. Comparison between Finite Element and Beam Equation: Percent difference in vertical displacement as a function of x (for the same crack length).

Figure 14. Comparison between Finite Element and Beam Equation: End load versus end displacement for 3 different Finite Element meshes. (The higher discrepancy at $\delta^*/h^* > 2.7$ is due to the coarse mesh region.)

Figure 15. The exponent N in the assumed power law $C = aI^N$ as a function of crack length for the propagating crack (material models 1, 3 and 4 as indicated).

PROBLEM DEFINITIONS

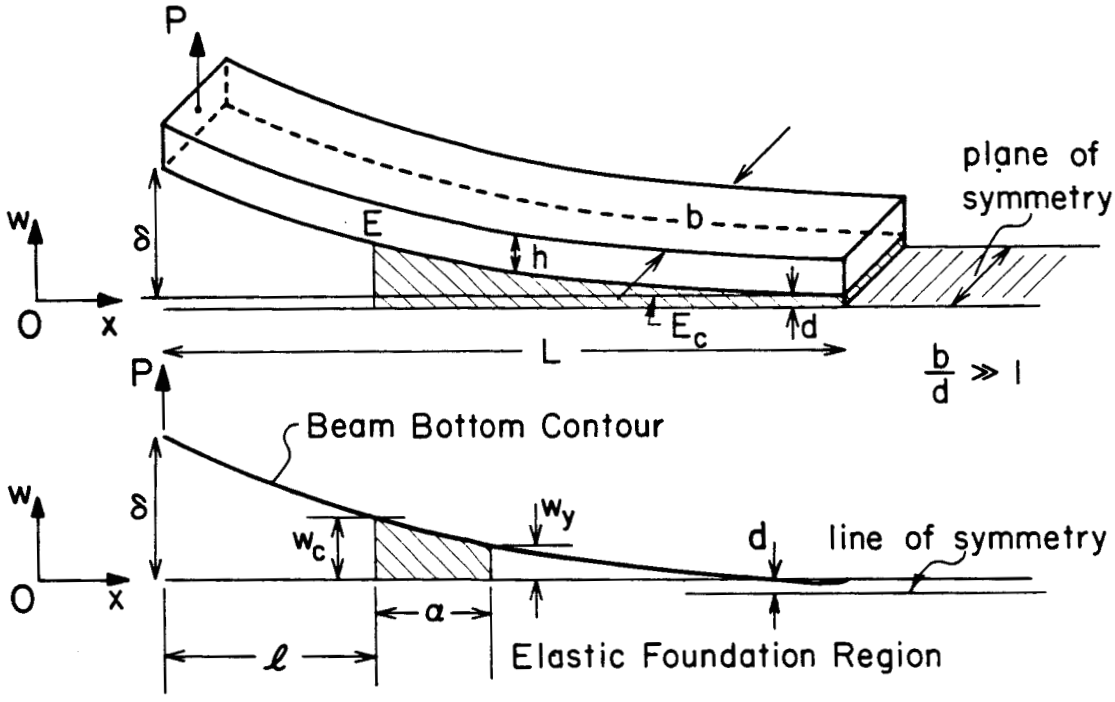

Material Model

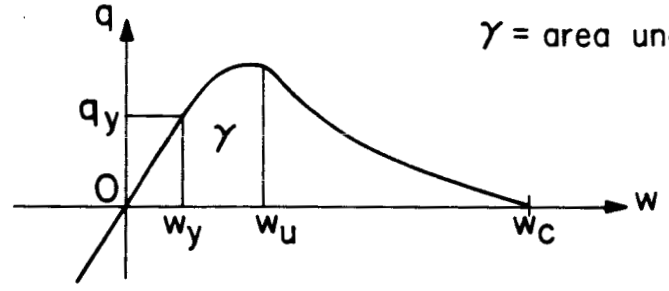

γ = area under q-w curve

E = Beam Modulus
E_c = Cohesive Elastic Modulus
p = End Load
δ = End Displacement
w = Vertical Displacement
ℓ = Crack Length
L = Beam Length
α = Yield Zone Size

h = Beam Height (thickness)
b = Beam Width
d = Cohesive Layer Thickness
q(w) = Cohesive Restoring Force
$w_y^* = \frac{w_y}{d}$ = Yield Strain
$w_u^* = \frac{w_u}{d}$ = Unloading Strain
$w_c^* = \frac{w_c}{d}$ = Critical (crack) Strain

Figure 1. Problem definition of the geometry and material parameters.

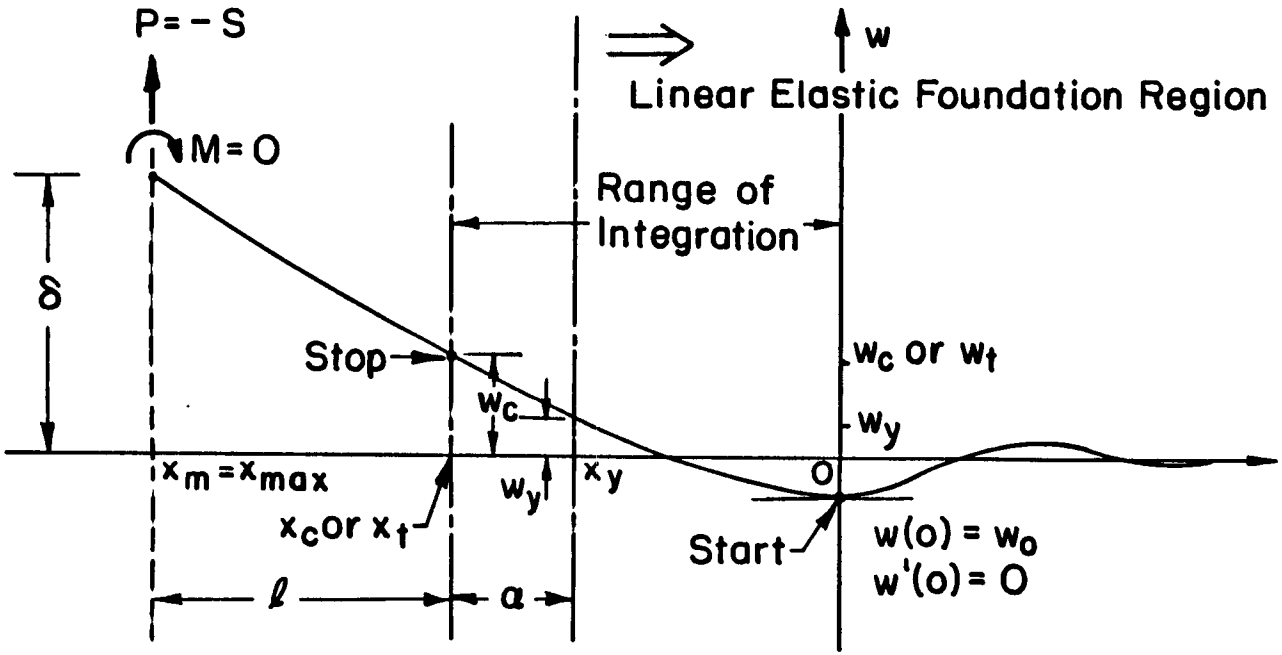

Figure 2. Solution schemes.

Material Models

(All models have the same γ^*)

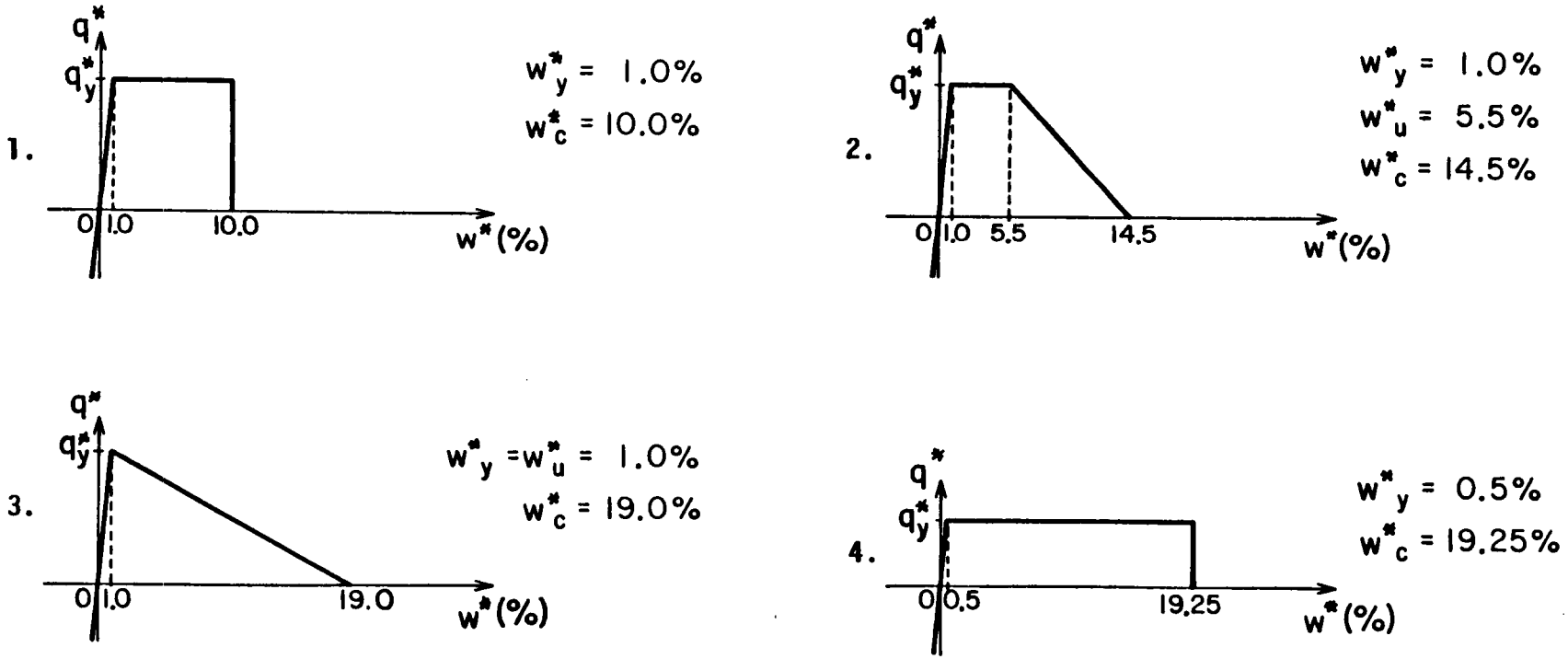

Figure 3. Material models (1, 2, 3 and 4).

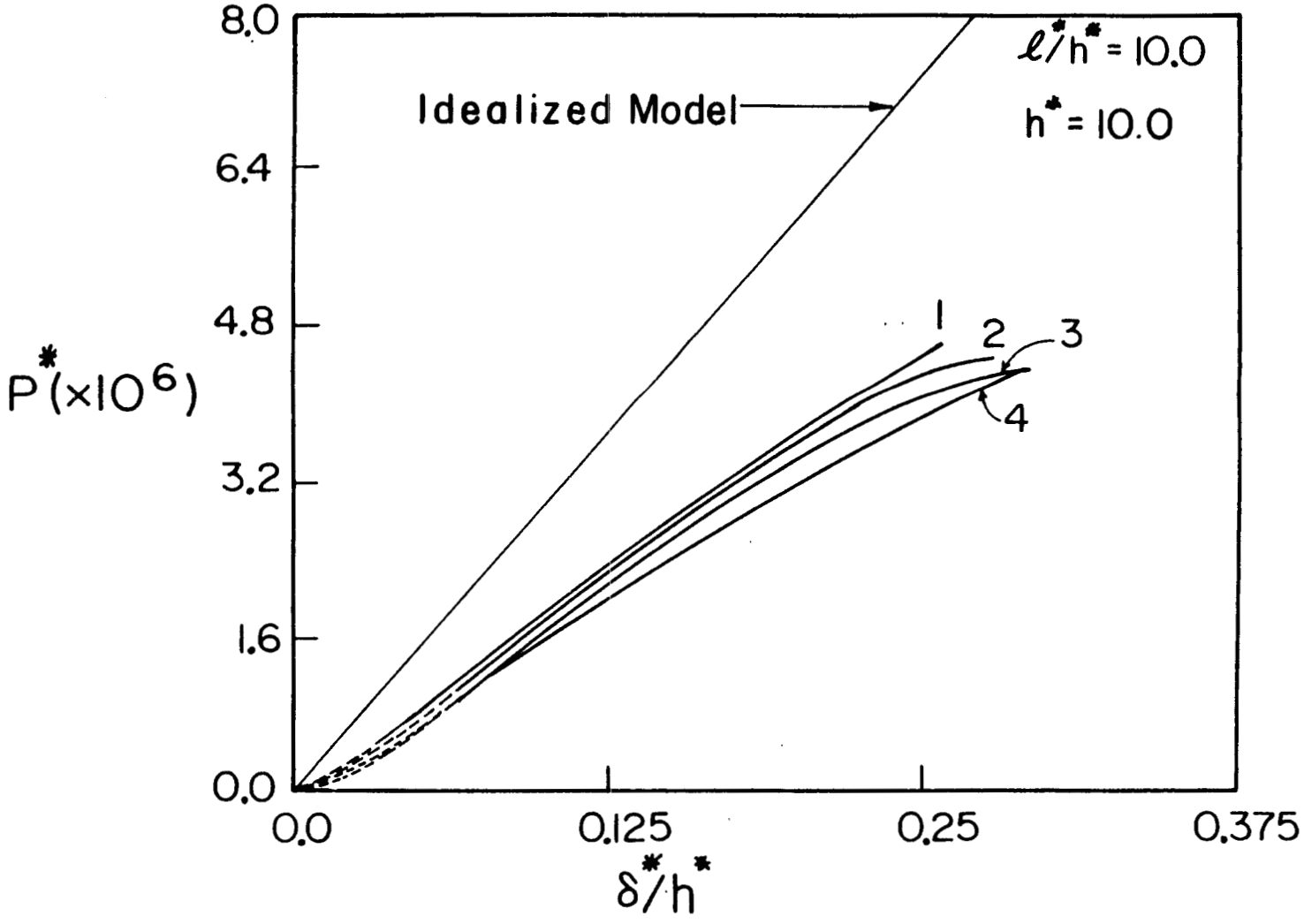

Figure 4. End load versus end displacement for the stationary crack (material models 1, 2, 3, and 4 as indicated). For explanation of the dashed portions of the P-δ curves see text.

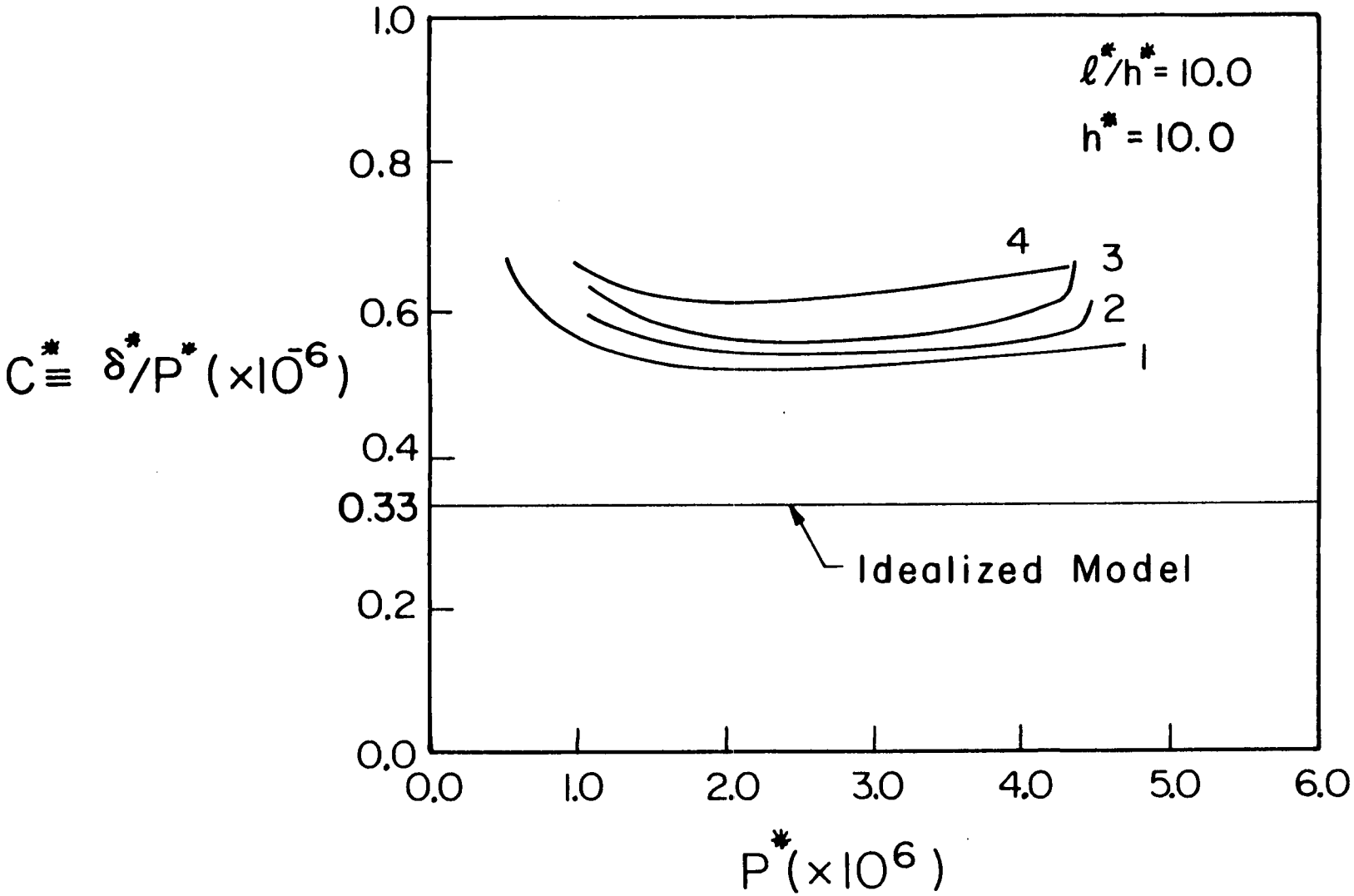

Figure 5. Compliance as a function of the end load for the stationary crack (material models 1, 2, 3 and 4 as indicated).

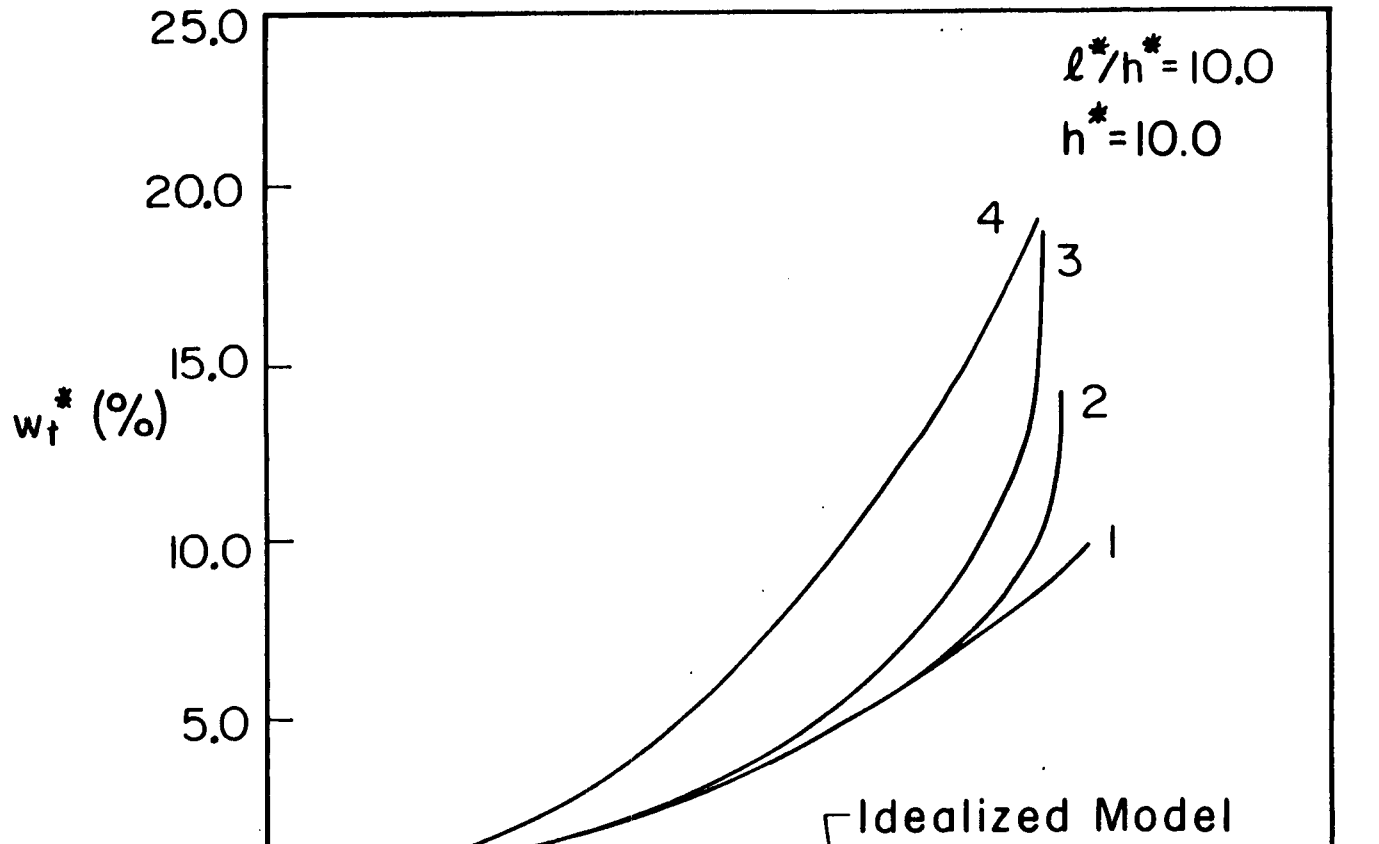

Figure 6. Crack tip displacement as a function of the end load for the stationary crack (material models 1, 2, 3 and 4 as indicated).

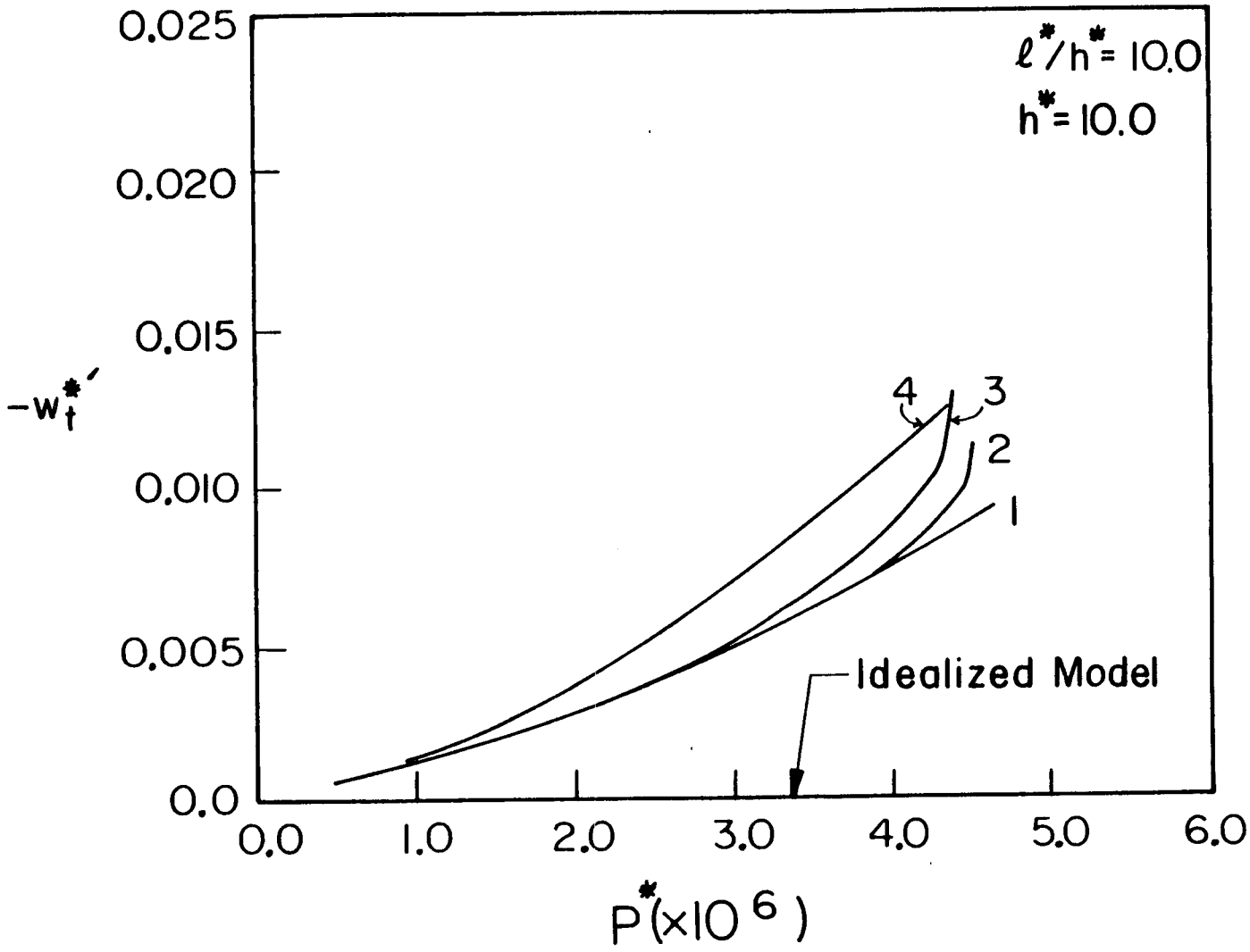

Figure 7. Slope at the crack tip as a function of the end load for the stationary crack (material models 1, 2, 3 and 4 as indicated).

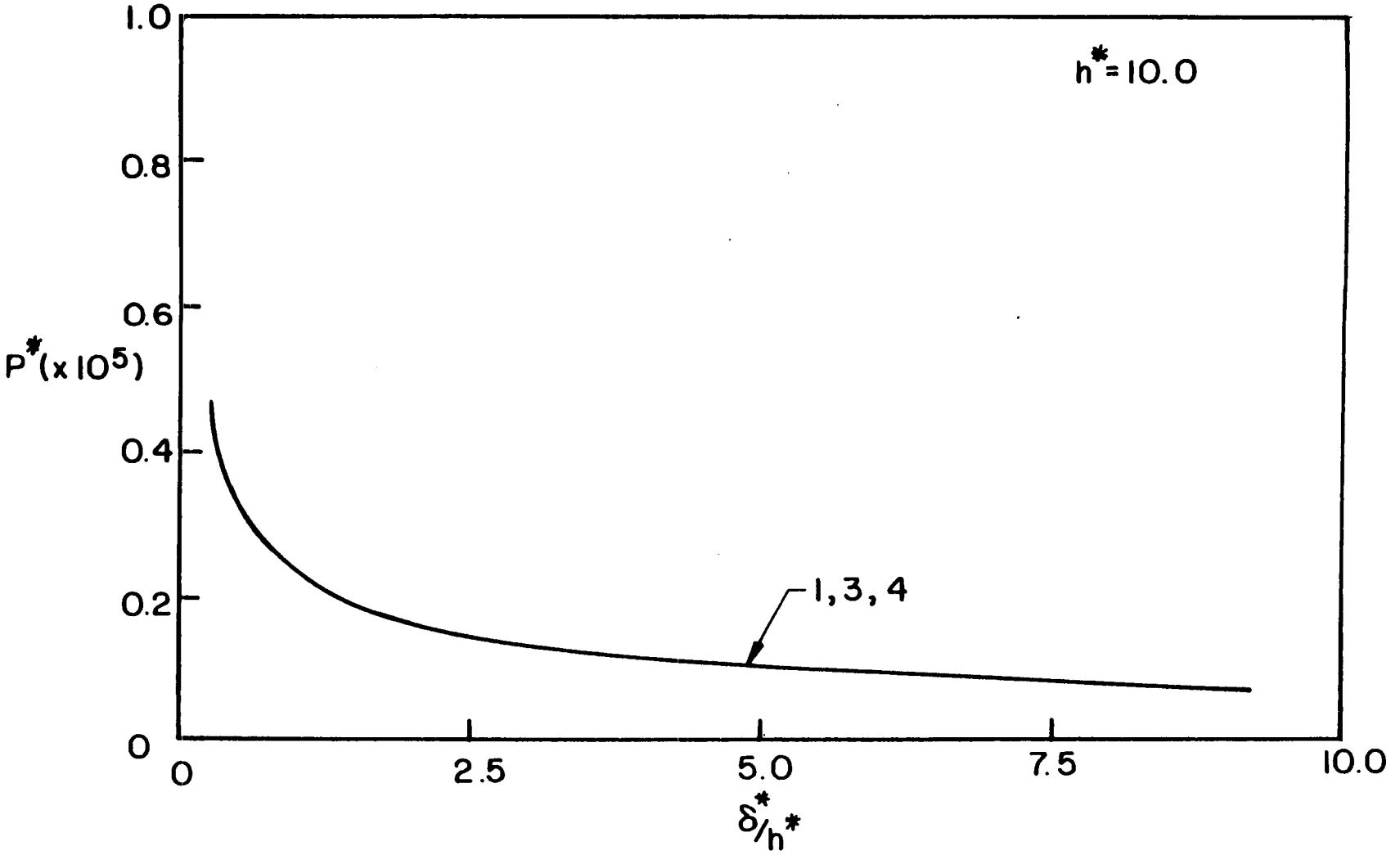

Figure 8. End load versus end displacement for the propagating crack (material models 1, 3 and 4 as indicated). Note that the relation displayed is not affected by the detailed characteristics of q(w).

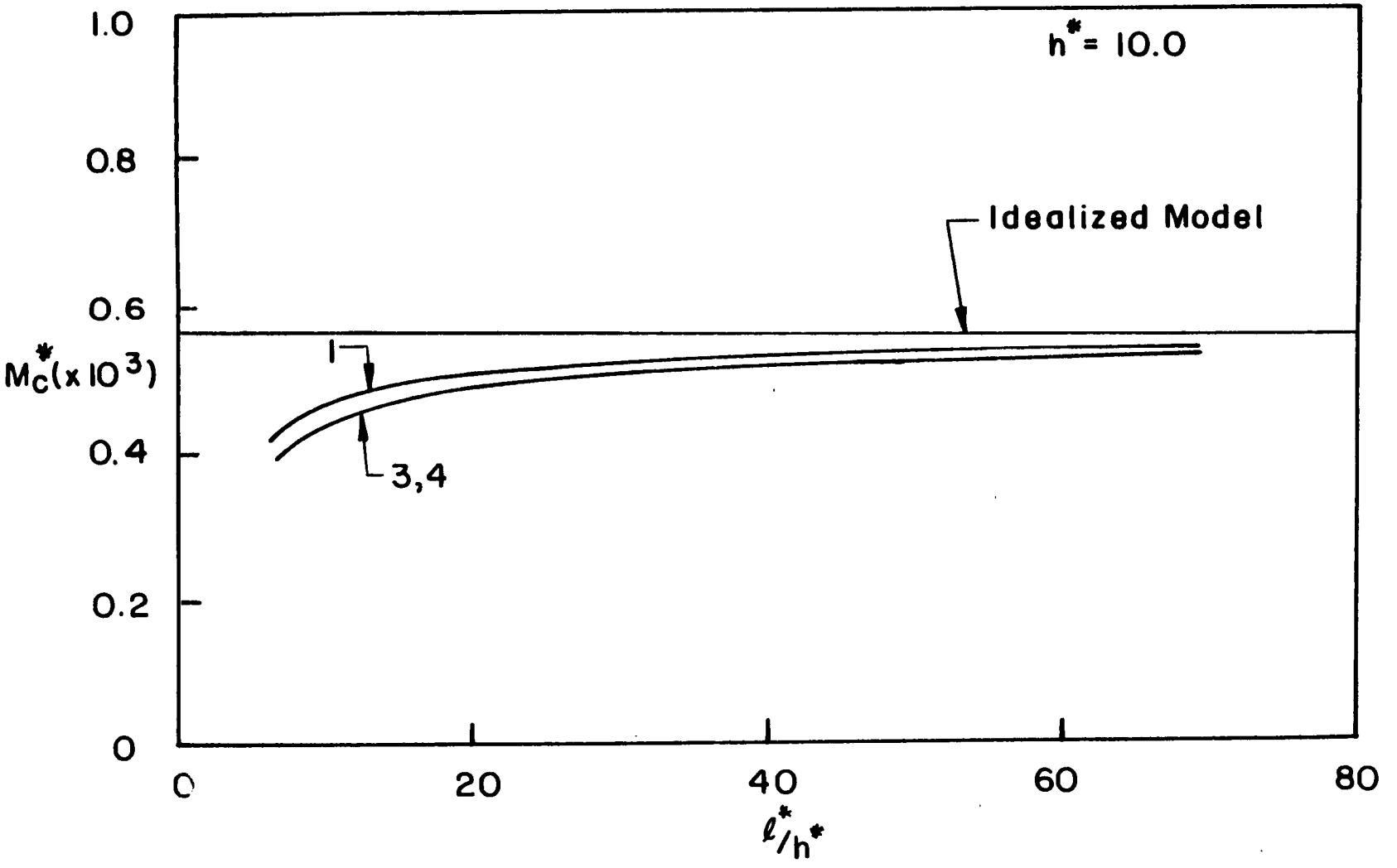

Figure 9. Moment at the crack tip as a function of crack length for the propagating crack (material models 1, 3 and 4 as indicated).

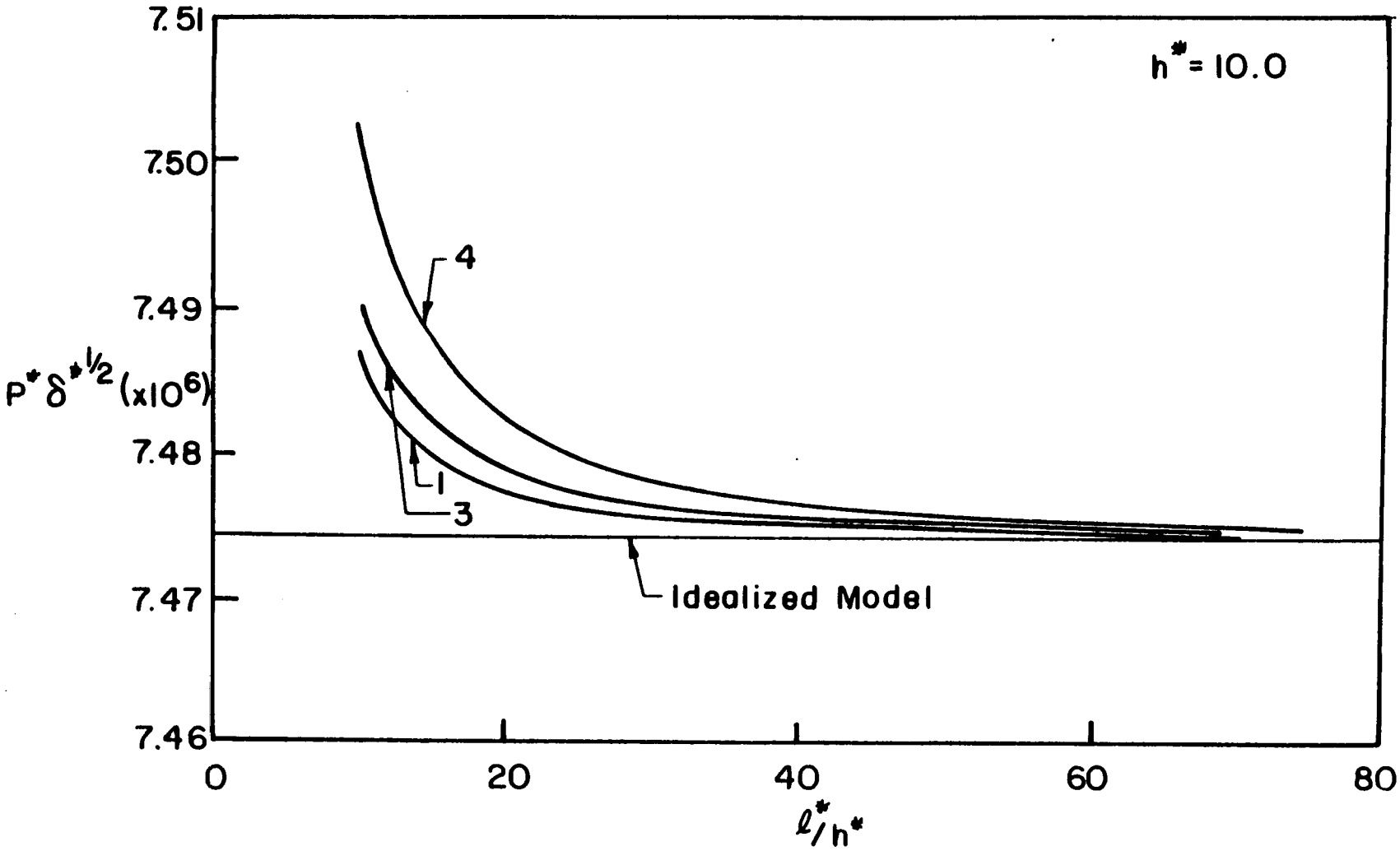

Figure 10. $P^*\delta^{*1/2}$ as a function of crack length for the propagating crack (material models 1, 3 and 4 as indicated).

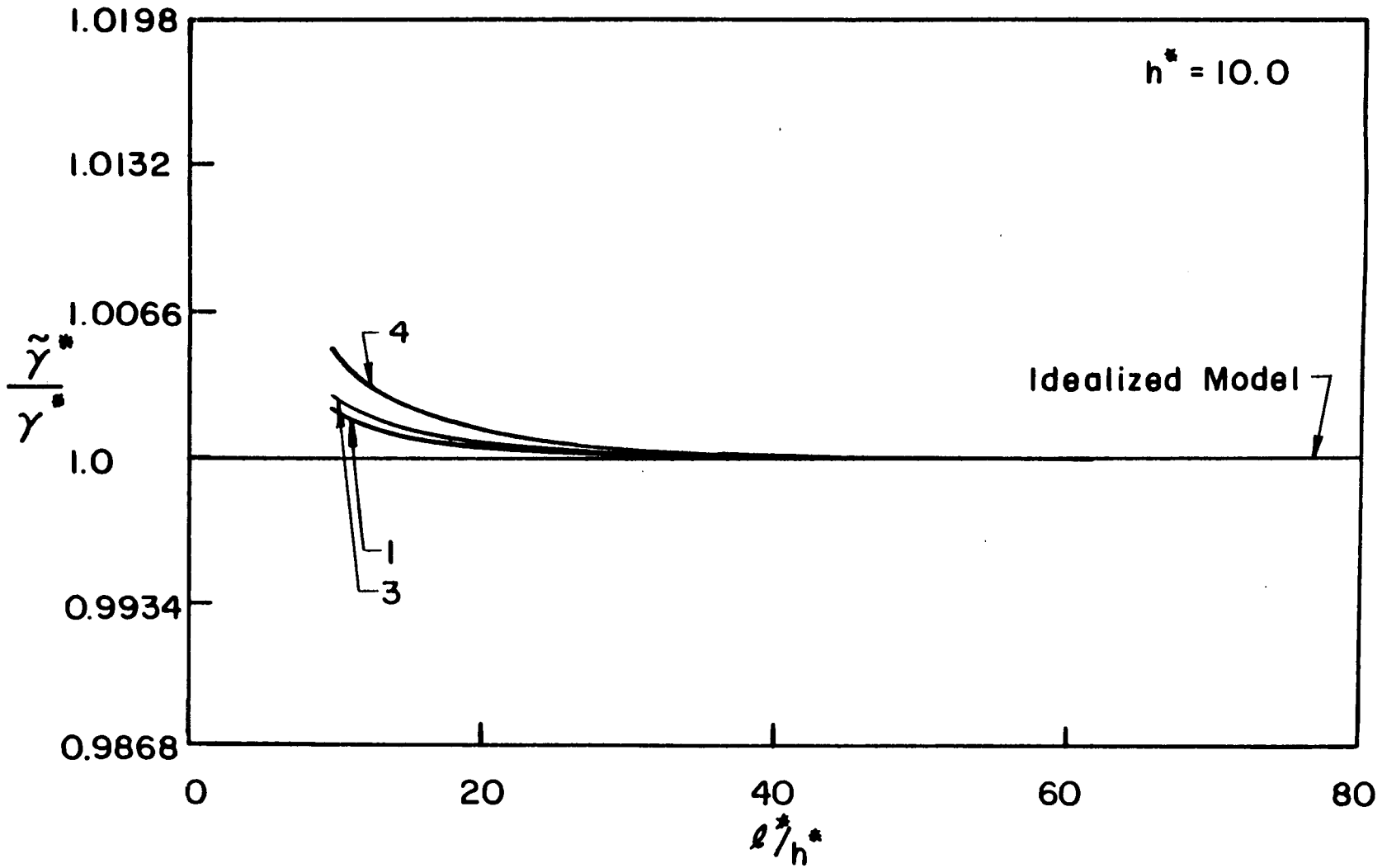

Figure 11. $\tilde{\gamma}^*/\gamma^*$ as a function of crack length for the propagating crack (Material models 1, 3 and 4 as indicated)

Beam on Nonlinear Cohesive Foundation

Finite Element Meshes

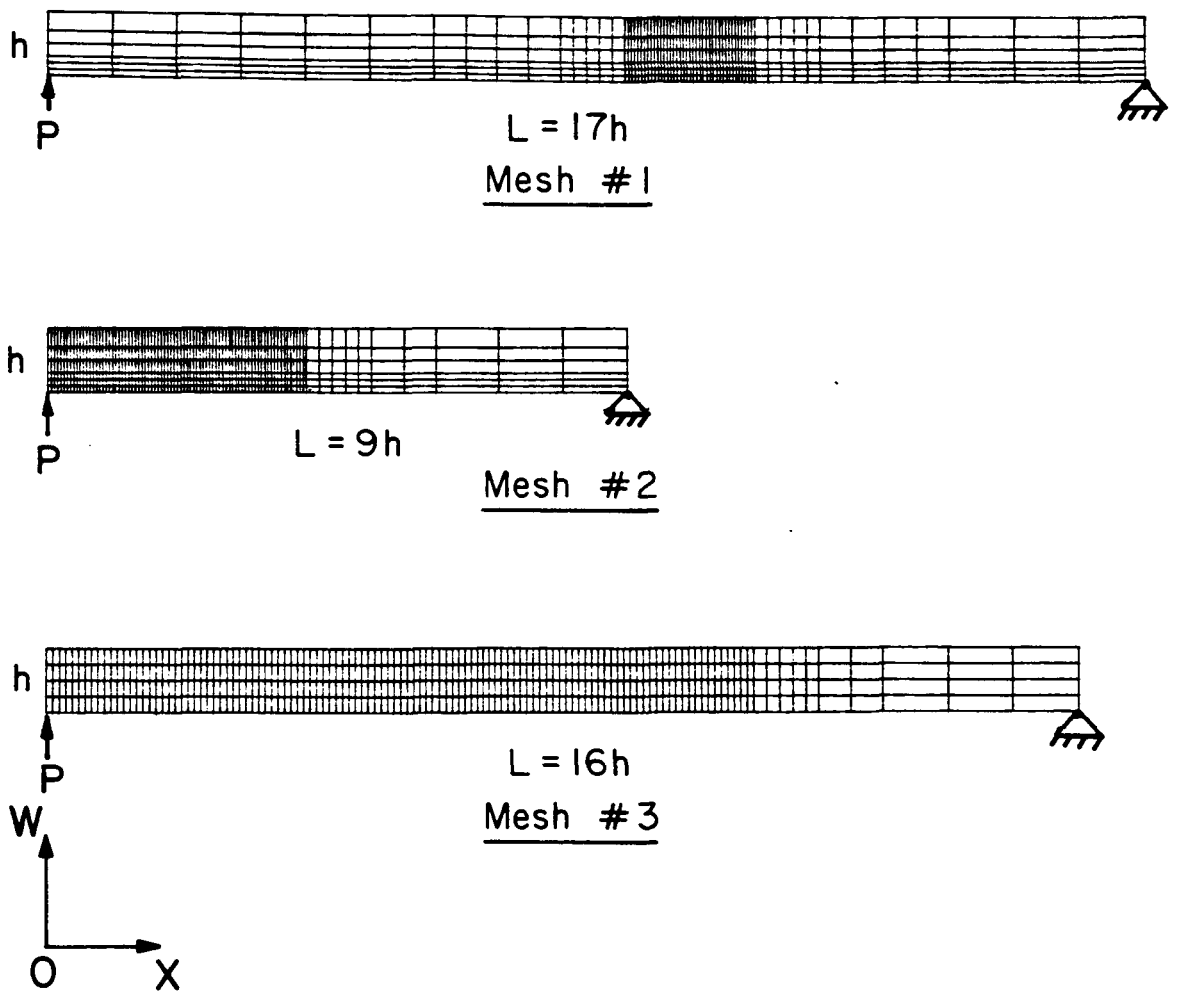

Figure 12. Finite element meshes.

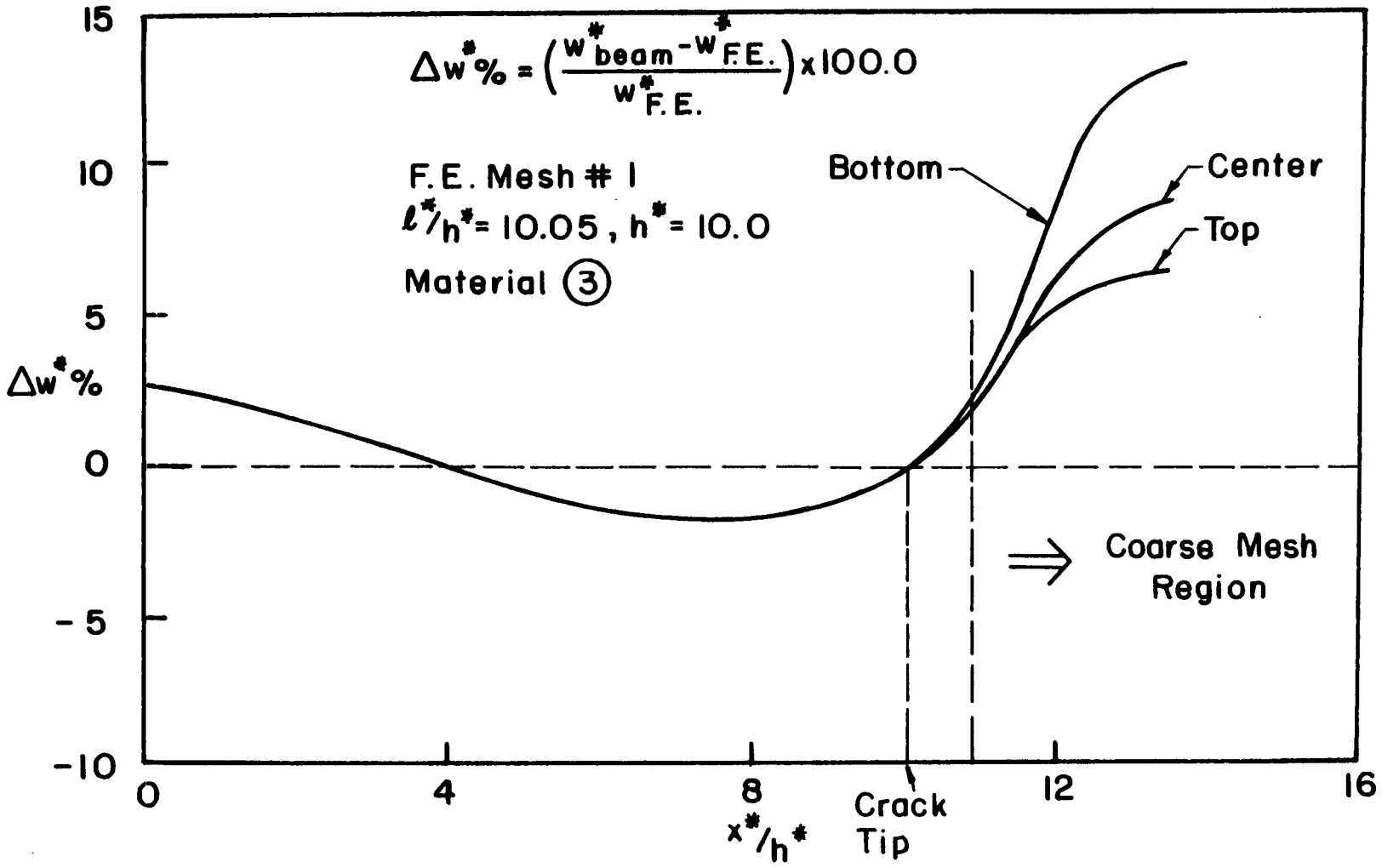

Figure 13. Comparison between Finite Element and Beam Equation: Percent difference in vertical displacement as a function of x (for the same crack length).

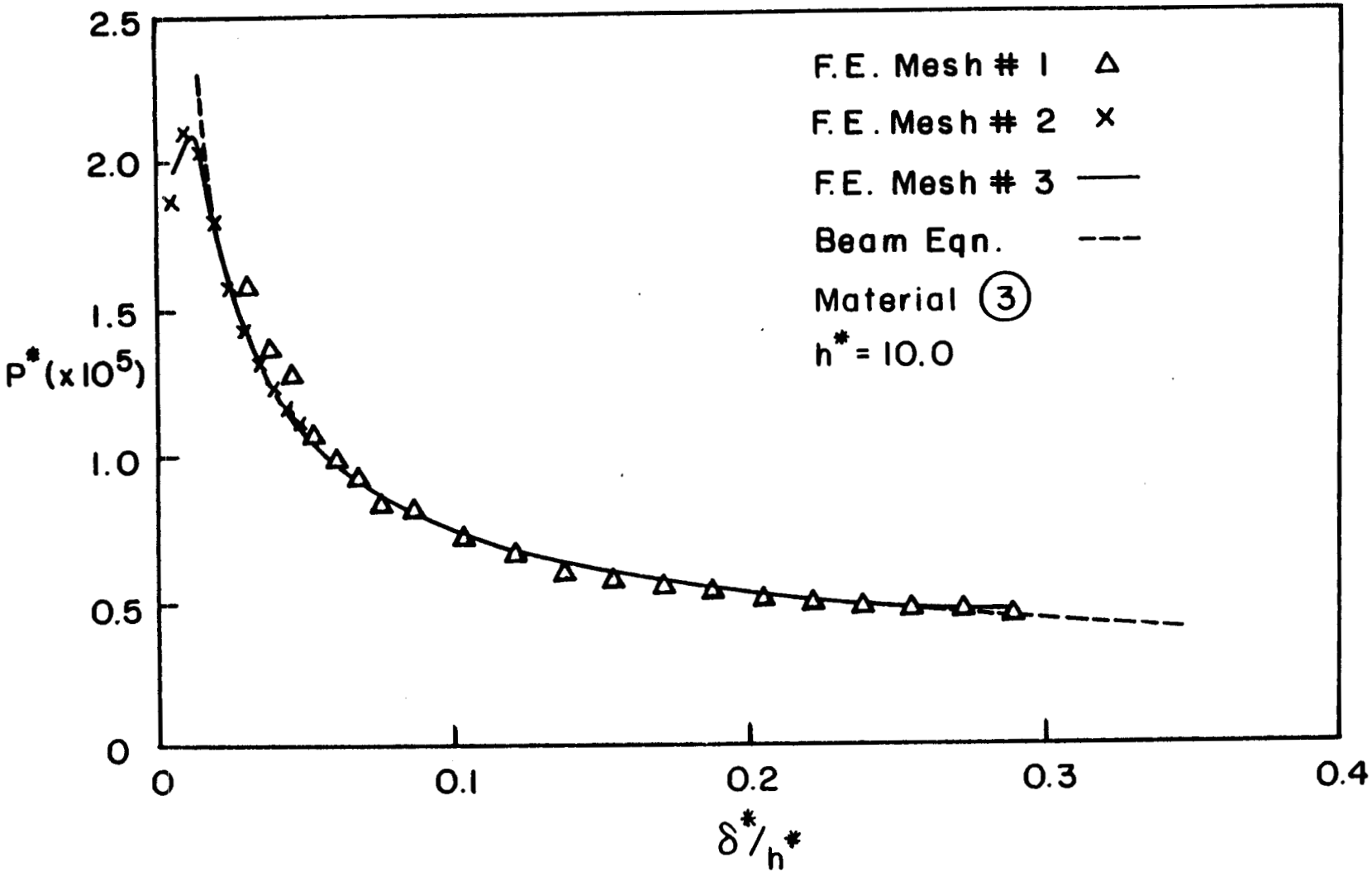

Figure 14. Comparison between Finite Element and Beam Equation: End load versus end displacement for 3 different Finite Element meshes. (The higher discrepancy at $\delta^*/h^* > 2.7$ is due to the coarse mesh region.)

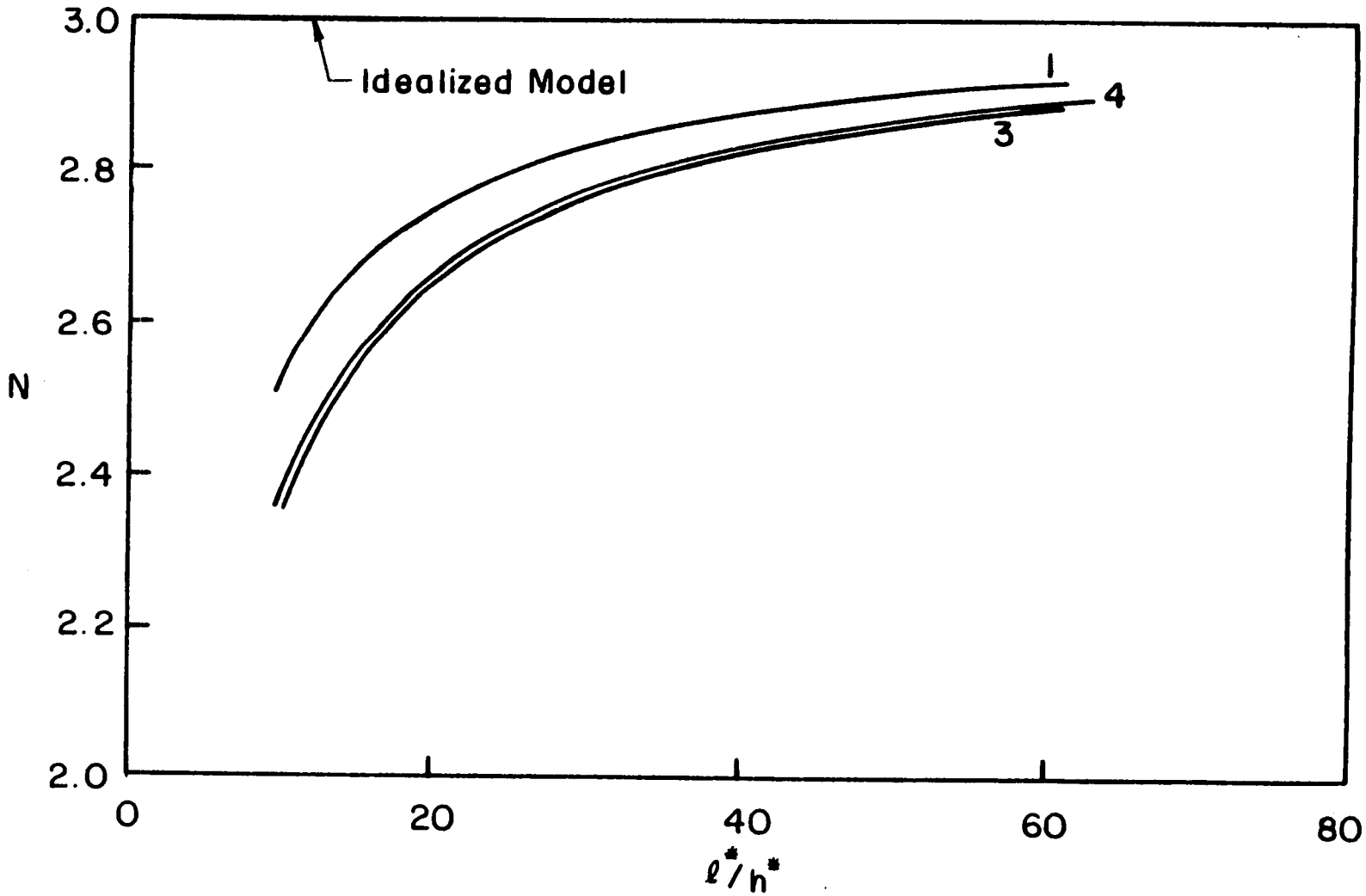

Figure 15. The exponent N in the assumed power law $C = al^N$ as a function of crack length for the propagating crack (material models 1, 3 and 4 as indicated).